(Received 18 March 2024, Accepted 19 June 2024, Scheduled 9 July 2024)

New THz Notch Filter Based on Cylindrical Periodic Structure

Tarik Touiss*, Mohammed R. Qasem, Siham Machichi, Farid Falyouni, and Driss Bria

Laboratory of Materials, Waves, Energy and Environment, Team of Waves, Acoustic, Photonic and Materials Faculty of Sciences, Mohamed First University, Oujda, Morocco

ABSTRACT: We propose and numerically analyze a new type of notch filter operating at terahertz frequencies, using a cylindrical periodic structure. This study takes place in the context of increasing demand for precise filtering devices in the terahertz frequency range, crucial for various applications in telecommunications, sensing, and medical field. This research focuses on the numerical analysis of the proposed structure, using the transfer matrix method to examine how changes in geometric parameters influence wave transmission. Particular attention is given to the effects introduced by the radii of the cylinders making up the structure. The principal results show that perfect symmetry (radii $R_1 = R_2$) produces no significant transmission dip, indicating the absence of resonance in the frequency band studied. This configuration allows the device to function as a passive filter. The introduction of asymmetry ($R_1 \neq R_2$) leads to the appearance of transmission dips, meaning that the device functions as a notch filter, capable of blocking specific frequencies. This phenomenon offers a method of selective filtering, by "activating" or "deactivating" the filter's behavior. Our research demonstrates the potential of the proposed cylindrical periodic structure as an innovative solution for the design of notch filters in the THz range. The ability to precisely control wave transmission through geometrical adjustments opens up new ways to develop highly selective filter devices adaptable to various technological applications.

1. INTRODUCTION

Terahertz (THz) waves, which occupy the spectral region between infrared and microwave frequencies, cover a range from 0.1 to 10 THz. They hold significant potential for applications in diverse fields such as biochemistry, security, pharmaceutical quality control, and wireless communications [1–4]. The main challenge in utilizing THz waves is finding low-loss materials that are transparent at these frequencies, with dry air being the most effective naturally occurring medium. To address this, free-space transmission of THz radiation has become a promising approach. Innovations in this area have led to the development of two primary types of waveguide structures for efficient THz wave propagation: surface-guiding waveguides [5] and hollow-core waveguides [6] with specialized cladding. The integration of functional THz devices into these waveguides could greatly improve system reliability and enable high-density integration, opening the door to more sophisticated and dependable THz technologies.

THz filters play a pivotal role in the manipulation of THz waves, with their ability to selectively transmit or block specific frequencies. This capability is crucial for enhancing dispersion in high-resolution THz imaging and for optimizing THz communication links [7–9]. Waveguide-based THz filters, noted for their stability and compactness, eliminate the need for bulky spatial components, making them ideal for integrated systems [10, 11]. For instance, THz filters utilizing one-dimensional photonic crystal waveguides have been shown to significantly increase gas detection sensitivity [12]. Similarly, two-dimensional photonic crystal cavity waveguides offer precise frequency selection, demonstrating their utility in THz filtering [10, 11].

Cylindrical waveguides are essential in many applications, especially for the efficient transmission of electromagnetic waves over long distances and at high frequencies [13]. They also represent a new generation of filtering technologies, proving to be highly beneficial for microwave circuits [14, 15]. The research by Gomez et al. [16] on photonic bandgap filters made from cylindrical waveguides with Kronig-Penney morphology highlights the tunability of these filters. By adjusting the Kronig-Penney parameters, they were able to control the bandgap and enhance filter performance, showcasing the potential of cylindrical waveguides in creating advanced photonic bandgap filters.

The selection of relative permittivity values ($\varepsilon_1 = 2.3$ and $\varepsilon_2 = 5$) in cylindrical waveguides simulations are crucial for enhancing the performance and efficiency of terahertz (THz) devices. Studies show that materials like polyethylene [17, 18], with its low-loss characteristics, and silicon nitride, used in quantum frequency combs [19] and photonic technologies [20], are optimal for THz applications due to their effective integration and operational efficiency at THz frequencies. This study shows that the ripples observed in the transmission spectra are mainly due to geometric discontinuities in the waveguide, which cause reflections and interferences. These ripples can be minimized by optimizing waveguide dimensions, periodicity, and material uniformity. To fabricate one-dimensional cylindrical periodic structures, techniques such as interference lithography, 3D printing, and femtosecond laser processing are used [21, 22].

* Corresponding author: Tarik Touiss (tariktouiss22@gmail.com).

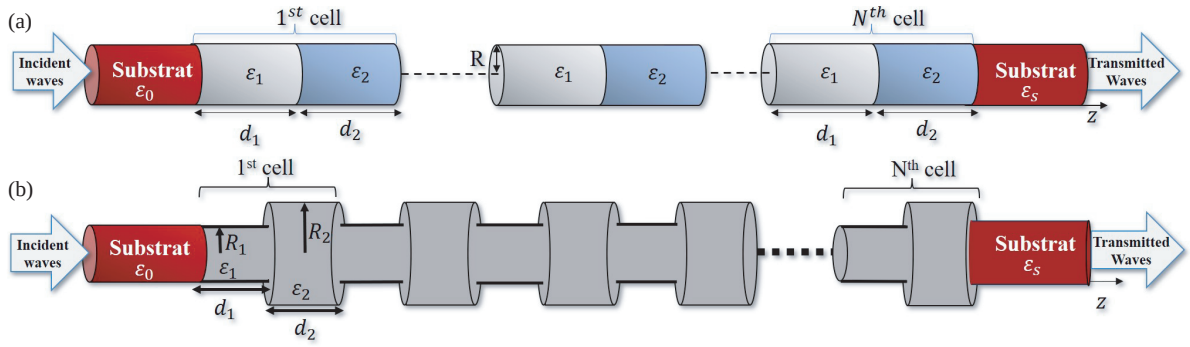

FIGURE 1. Geometrical scheme of 1D periodic cylindrical waveguide structure formed by alternating two periodic cylindrical waveguides of lengths d_1 and d_2 and permittivity ε_1 and ε_2.

In our research, we employ the transfer matrix method (TMM) [23–26] to analyze the transmission rates of TEz and TMz modes in a one-dimensional cylindrical periodic structure. This structure alternates between two types of cylindrical waveguides, each made from different dielectric materials in direct contact (see Fig. 1).

The paper is structured as follows. Firstly, we provide a general introduction in Section 1. In Section 2, we present our analytical method of the transfer matrix for our structure, and then the transmission rate of the structure for the two propagation modes TEz and TMz. Moving on to Section 3, we present the numerical results for our system. Finally, we conclude our paper in Section 4.

2. ANALYTICAL METHOD

This study presents a formulation of Maxwell's wave equations in cylindrical coordinates. We consider the propagation of waves through a dielectric medium, characterized by its relative permittivity (ε_i) and relative permeability (μ_i), where 'i' represents the medium ($i = 1$ or $i = 2$). In cylindrical coordinates (r, φ, z), Maxwell's equations lead to the following equation for the E_z component of the electric field:

$$\left(\nabla^2 + \varepsilon_i \mu_i \frac{\omega^2}{c^2}\right) E_z\left(r, \varphi, z\right) = 0 \tag{1}$$

The general solution for $E_z(r, \varphi, z)_i$, corresponding to a specific value of n, is expressed as:

$$E_z(r, \varphi, z)_i = \left\{A_{(i)} \left(\gamma_{nm}^{(i)}\right)^2 e^{ik_{nm}^{(i)} z} + B_{(i)} \left(\gamma_{nm}^{(i)}\right)^2 e^{-ik_{nm}^{(i)} z}\right\} J_n\left(\frac{x_{nm}}{R} r\right) \cos(n\varphi) \tag{2}$$

Here, the relation between $\gamma_{nm}^{(i)}$ and $k_{nm}^{(i)}$ is defined as:

$$\left(k_{nm}^{(i)}\right)^2 = \varepsilon_i \mu_i \frac{\omega^2}{c^2} - \left(\gamma_{nm}^{(i)}\right)^2 = \varepsilon_i \mu_i \frac{\omega^2}{c^2} - \left(\frac{x_{nm}}{R}\right)^2 \tag{3}$$

Equation (3) indicates that for a given angular frequency ω, $k_{nm}^{(i)}$ is real for the first x_{nm} roots of the Bessel function, allowing wave propagation. Conversely, higher order values of x_{nm} at the same frequency lead to an imaginary $k_{nm}^{(i)}$, causing wave attenuation. We focus on the TM_{01} and TE_{11} modes in cylindrical guides, with n and m values starting at 0 and 1, respectively. The cut-off frequency, where the longitudinal propagation constant becomes zero, is:

$$f_c = \frac{c}{\sqrt{\varepsilon_i \mu_i}} \frac{x_{nm}}{2\pi R} \tag{4}$$

Considering the field components parallel and transverse to the z-axis:

$$\overrightarrow{E}\left(r, \varphi, z\right) = \overrightarrow{E_z}\left(r, \varphi, z\right) + \overrightarrow{E_t}\left(r, \varphi, z\right) \tag{5}$$

We analyze electromagnetic wave propagation in cylindrical waveguides with uniform cross-sections. Maxwell's equations, combined with an explicit zone dependency, allow transverse fields to be determined from axial components. For TE_{nm} and TM_{nm} modes, the transverse components relate as follows:

- For TE_{nm} modes:

$$\overrightarrow{B_t}\left(r, \varphi, z\right)_i = \overrightarrow{\nabla_t}\left\{\frac{1}{\gamma_{nm}^2} \frac{\partial B_z\left(r, \varphi, z\right)_i}{\partial z}\right\} \tag{6a}$$

$$\overrightarrow{E_t}\left(r, \varphi, z\right)_i = -\frac{i\omega}{c} \overrightarrow{e_z} \times \overrightarrow{\nabla_t}\left\{\frac{1}{\gamma_{nm}^2} B_z\left(r, \varphi, z\right)_i\right\} \tag{6b}$$

- For TM_{nm} modes:

$$\overrightarrow{E_t}\left(r, \varphi, z\right)_i = \overrightarrow{\nabla_t}\left\{\frac{1}{\gamma_{nm}^2} \frac{\partial E_z\left(r, \varphi, z\right)_i}{\partial z}\right\} \tag{6c}$$

$$\overrightarrow{B_t}\left(r, \varphi, z\right)_i = \frac{i\varepsilon_i \mu_i \omega}{c} \overrightarrow{e_z} \times \overrightarrow{\nabla_t}\left\{\frac{1}{\gamma_{nm}^2} E_z\left(r, \varphi, z\right)_i\right\} \tag{6d}$$

Continuity conditions at the $z = \bar{z}$ ($\bar{z} = 0$, d_1 and $d_1 + d_2$) discontinuity require the transverse components $\overrightarrow{E_t}$ and $\overrightarrow{B_t}$ of the electric and magnetic fields to be continuous as:

$$\begin{cases} \overrightarrow{E_t}\left(r, \varphi, z\right)_1 \Big|_{z=\bar{z}} = \overrightarrow{E_t}\left(r, \varphi, z\right)_2 \Big|_{z=\bar{z}} \\ \overrightarrow{B_t}\left(r, \varphi, z\right)_1 \Big|_{z=\bar{z}} = \overrightarrow{B_t}\left(r, \varphi, z\right)_2 \Big|_{z=\bar{z}} \end{cases} \tag{7}$$

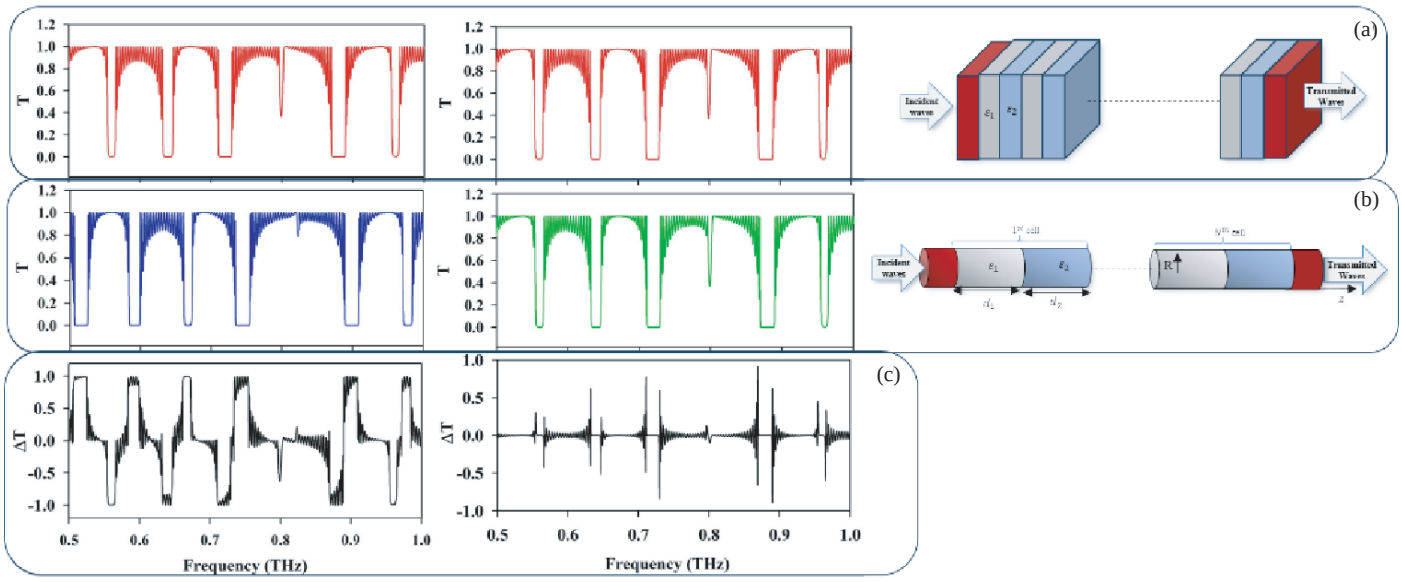

FIGURE 2. Variation of the transmission rate as a function of the frequency (THz) for different systems, with $d_1 = d_2 = 500\,\mu\text{m}$, $\varepsilon_1 = 2.3$ and $\varepsilon_2 = 5$.

The transfer matrix for a cell composed of two cylindrical waveguides is derived from these conditions:

$$\begin{pmatrix} 1 & 1 \\ \alpha_0 & -\alpha_0 \end{pmatrix} \begin{pmatrix} A_0 \\ B_0 \end{pmatrix} = A_1 \begin{pmatrix} T_{11} & T_{12} \\ T_{21} & T_{22} \end{pmatrix} \begin{pmatrix} 1 \\ \alpha_s \end{pmatrix} = A_1 M_{cell} \begin{pmatrix} 1 \\ \alpha_s \end{pmatrix} \quad (8)$$

For a system comprising N cells (as illustrated in Fig. 1), the transfer matrix of the periodic structure is obtained by matrix multiplication:

$$\begin{pmatrix} A_0 \\ B_0 \end{pmatrix} = \begin{pmatrix} T_{11} & T_{12} \\ T_{21} & T_{22} \end{pmatrix} \begin{pmatrix} A_1 \\ B_1 \end{pmatrix} = \begin{pmatrix} T_{11} & T_{12} \\ T_{21} & T_{22} \end{pmatrix}^2 \begin{pmatrix} A_2 \\ B_2 \end{pmatrix} = \begin{pmatrix} T_{11} & T_{12} \\ T_{21} & T_{22} \end{pmatrix}^N \begin{pmatrix} A_N \\ B_N \end{pmatrix} \quad (9)$$

The N^{th} order unit matrix is simplified to:

$$\begin{pmatrix} T_{11} & T_{12} \\ T_{21} & T_{22} \end{pmatrix}^N = \begin{pmatrix} M_{11} & M_{12} \\ M_{21} & M_{22} \end{pmatrix} \quad (10)$$

Finally, the transmission rate of the structure is calculated as:

$$T = \left| \frac{2}{\left[M_{11} + \alpha_s M_{12} + \frac{M_{21}}{\alpha_0} + M_{22} \left(\frac{\alpha_s}{\alpha_0} \right) \right]} \right|^2 \quad (11)$$

3. RESULTS AND DISCUSSIONS

In this section, we present numerical simulations of the transmission spectra for a novel notch filter designed for terahertz (THz) frequency applications. The filter is based on a cylindrical periodic structure characterized by a unit cell that repeats along the propagation axis. Each cell is composed of two cylindrical dielectric waveguides with respective lengths d_1 and d_2, and the total period is defined as $d = d_1 + d_2$. The waveguides are characterized by different relative permittivity values, with $\varepsilon_1 = 2.3$ and $\varepsilon_2 = 5$, and they share a common radius R, as illustrated in Fig. 1(a). In another configuration, the waveguides have different radii, R_1 and R_2, but the same relative permittivity $\varepsilon_1 = \varepsilon_2 = 2.3$, as shown in Fig. 1(b). The structure comprises $N = 20$ cells.

3.1. Comparative Study between Two Systems

Fig. 2 shows transmission spectra (T) for different optical or electromagnetic systems across a range of terahertz (THz) frequencies. Each sub-figure illustrates the effect of system geometry on wave transmission. (a) The lamellar system is illustrated, where the spectra in red correspond to this system. (b) The cylindrical system is shown, where the blue and green spectra represent cylindrical systems with radii of 250 micrometers and 10,000 micrometers, respectively. It can be seen that the spectrum changes with the radius of the cylinder. This indicates that cylinder size influences the distribution and bandwidth of the transmission spectrum. (c) The spectra in black show the difference (ΔT) between the lamellar and cylindrical systems. These difference spectra are obtained by subtracting the transmission values of the lamellar system from those of the cylindrical system. The results show significant variations, indicating that the transmission of a wave through a system is highly dependent on its geometry. Positive values of ΔT suggest frequencies where the lamellar system transmits better than the cylindrical system, and vice versa for negative values. We also observe that the difference between lamellar and cylindrical systems becomes negligible when the radius R of the cylin-

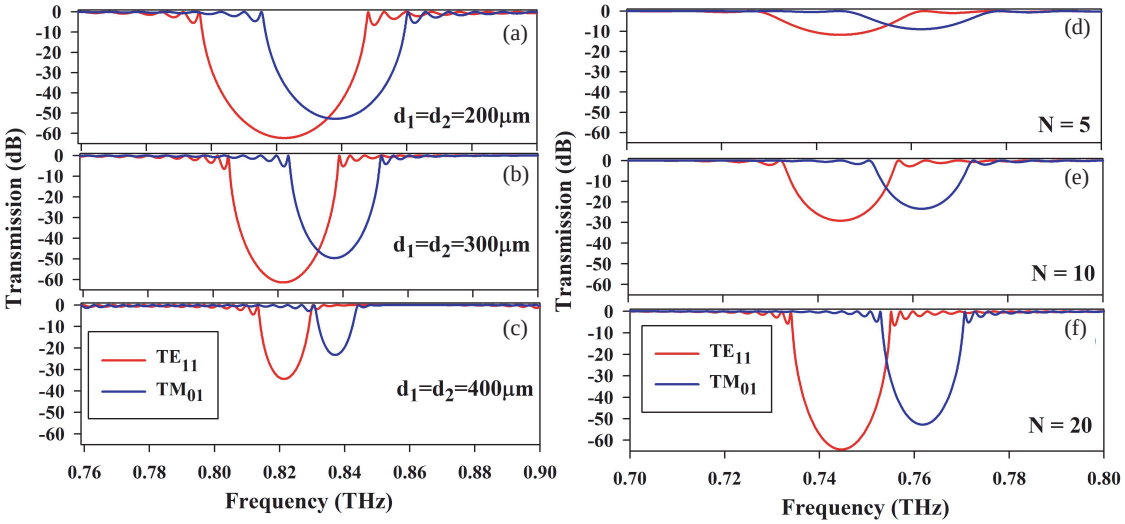

FIGURE 3. Variation of the transmission (dB) as a function of the frequency (THz), with ((a) to (c)) different values of $d_1 = d_2$, ((d) to (f)) different N. In all cases, we have fixed the radius ($R = 250$ µm).

drical system is very large. This suggests that, in the limit where R tends towards infinity, the behavior of the cylindrical system approaches that of the lamellar system.

3.2. Influence of the Structural Parameters

In this part, we analyze the selection of the structural parameters of the filter and study the impact of these parameters on the transmission spectra, specifically for two modes TE_{11} (red line) and TM_{01} (blue line) of the proposed system.

When values of R and N are fixed as 250 µm and 20, we explore the transmission spectra for different $d_1 = d_2$ values (200 µm, 300 µm and 400 µm), as shown in Figs. 3(a) to 3(c). These figures demonstrate how altering $d_1 = d_2$ affects the filter's transmission properties. As $d_1 = d_2$ increases, we observe that the transmission minima, or the points of strongest absorption/reflection, remain constant in frequency. However, there is a noticeable narrowing of the filter's bandwidth. This reduction in bandwidth enhances the filter's selectivity, allowing it to isolate a more precise frequency range.

Further analysis is presented in Figs. 3(d) to 3(f), which illustrate the effects of varying N (5, 10, and 20) while keeping $d_1 = d_2$ constant at 500 µm. Increasing N makes the transmission minima more pronounced, yet does not alter their frequency or bandwidth. This indicates that N significantly boosts the filter's ability to attenuate signals at specific frequencies, enhancing its efficiency in blocking or dampening unwanted waves. The increased attenuation, reflected in more negative decibel (dB) values, underscores the filter's improved performance in creating distinct passbands and stopbands.

In this analysis, we study the impact of filter radius on the transmission characteristics of optical filters, focusing on two transmission modes: TE_{11} and TM_{01}. Figs. 4(a), 4(b), and 4(c) show transmission levels in decibels (dB) at different frequencies (THz), with each figure corresponding to a different filter radius (R). A key observation from these figures is the shift of deep transmission valleys to lower frequencies as the filter radius increases from 250 µm to 450 µm. This shift indicates that the physical size of the filter significantly influences its resonance and transmission properties, with larger filters resonating at lower frequencies.

Figure 4(d), which shows the resonant frequency as a function of filter radius R for the TE_{11} and TM_{01} modes. The red and blue dots represent the TE_{11} and TM_{01} modes, respectively, and illustrate a clear trend of decreasing frequency with increasing radius. This trend confirms that larger structures tend to resonate at lower frequencies. Furthermore, as the radius increases, the resonant frequencies of the two modes converge, suggesting that physical changes in the filter structure have a differential impact on each mode. However, these differences decrease as the filter size increases, leading to closer resonance frequencies between the two modes.

3.3. Exploring the Influence of Radius R_2

This subsection investigates the effects of varying the cylindrical radius R_2 on the transmission spectrum, as shown in Fig. 1(b), focusing on its implications for the design of optical and communication devices. The ability to precisely control the transmission of specific frequencies is a cornerstone of the development of such systems. Fig. 5 shows the transmission spectrum for the TE_{11} propagation mode, illustrating how changes in the R_2 radius (while keeping the other parameters constant: $d_1 = d_2$ at 500 µm, R_1 at 250 µm, and both ε_1 and ε_2 at 2.3) influence the attenuation characteristics of the system.

In the case where $R_1 = R_2$, no transmission dip is observed (i.e., no significant resonance within the studied frequency band), this could indicate that the symmetry between the two cylinders results in a propagation mode where there is no marked attenuation. On the other hand, when R_2 differs from R_1, the introduced asymmetry could disrupt wave propagation in such a way that resonance is established, creating a transmission trough.

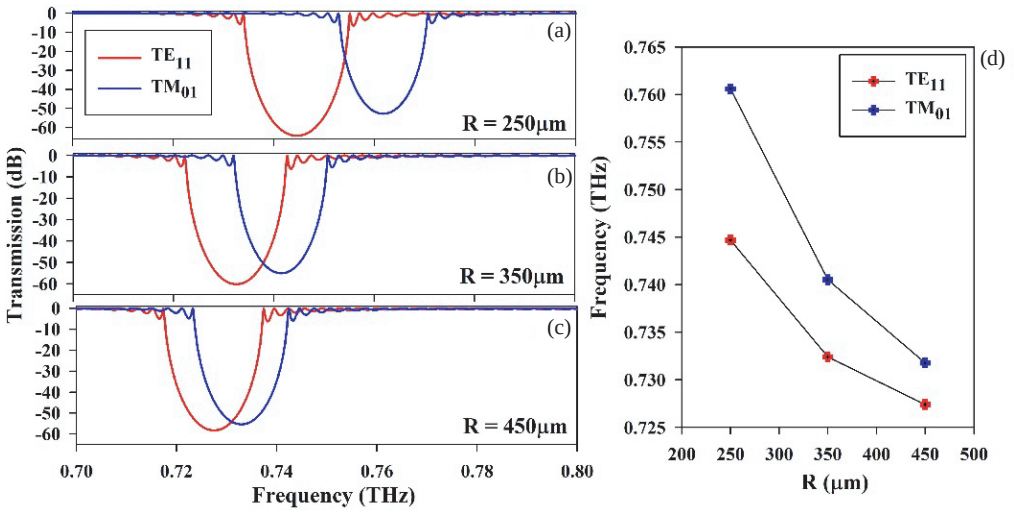

FIGURE 4. Variation the transmission (dB) as a function of frequency (THz) for different values of radius R (μm), with $d_1 = d_2 = 500$ μm, $\varepsilon_1 = 2.3$ and $\varepsilon_2 = 5$.

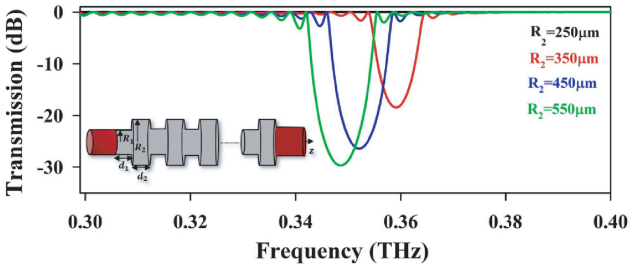

FIGURE 5. Transmission (dB) of TE_{11} propagation mode as a function of frequency (THz) for different values of radius R_2, with $d_1 = d_2 = 500$ μm, $R_1 = 250$ μm, and $\varepsilon_1 = \varepsilon_2 = 2.3$.

In the context of filter design, this property is exploited as follows: When $R_1 = R_2$, the device operates as a passive filter, where no frequency is specifically cut off in the range under study. When R_2 is different from R_1, the device operates as a notch filter, creating transmission dips at specific frequencies that are blocked. This ability to "activate" or "deactivate" notch filtering behavior by adjusting the relative radii of the cylinders offers a powerful tool for designing highly selective filtering systems.

4. CONCLUSION

Our study introduced and numerically analyzed a new notch filter based on a cylindrical periodic structure, marking a significant advance in terahertz frequency filtering technologies. By exploiting the interaction between the geometric parameters of the structure, notably the radii of the cylinders, we demonstrated the ability to selectively manipulate wave transmission through the filter. The results highlight two distinct operating regimes: passive filter behavior when the cylinders are symmetrical and notch filter behavior with the introduction of asymmetry. In sum, our work contributes to expanding the field of possibilities for the design and optimization of terahertz filtering devices.

REFERENCES

[1] Horiuchi, N., "Searching for terahertz waves," *Nature Photonics*, Vol. 4, No. 9, 662–662, 2010.

[2] Panwar, A. K., A. Singh, A. Kumar, and H. Kim, "Terahertz imaging system for biomedical applications: Current status," *System*, Vol. 28, 44, 2013.

[3] Zhao, H., K. Zhao, and R. Bao, "Fuel property determination of biodiesel-diesel blends by terahertz spectrum," *Journal of Infrared, Millimeter, and Terahertz Waves*, Vol. 33, 522–528, 2012.

[4] Webber, J., Y. Yamagami, G. Ducournau, P. Szriftgiser, K. Iyoda, M. Fujita, T. Nagatsuma, and R. Singh, "Terahertz band communications with topological valley photonic crystal waveguide," *Journal of Lightwave Technology*, Vol. 39, No. 24, 7609–7620, 2021.

[5] Wang, K. and D. M. Mittleman, "Metal wires for terahertz wave guiding," *Nature*, Vol. 432, No. 7015, 376–379, 2004.

[6] Li, H., S. Atakaramians, R. Lwin, X. Tang, Z. Yu, A. Argyros, and B. T. Kuhlmey, "Flexible single-mode hollow-core terahertz fiber with metamaterial cladding," *Optica*, Vol. 3, No. 9, 941–947, 2016.

[7] Gao, X., L. Zhou, X. Y. Yu, W. P. Cao, H. O. Li, H. F. Ma, and T. J. Cui, "Ultra-wideband surface plasmonic Y-splitter," *Optics Express*, Vol. 23, No. 18, 23 270–23 277, 2015.

[8] Lu, J.-T., C.-H. Lai, T.-F. Tseng, H. Chen, Y.-F. Tsai, Y.-J. Hwang, H.-C. Chang, and C.-K. Sun, "Terahertz pipe-waveguide-based directional couplers," *Optics Express*, Vol. 19,

No. 27, 26 883–26 890, 2011.

[9] Bingham, A. L. and D. Grischkowsky, "Terahertz two-dimensional high-Q photonic crystal waveguide cavities," *Optics Letters*, Vol. 33, No. 4, 348–350, 2008.

[10] Yee, C. M. and M. S. Sherwin, "High-Q terahertz microcavities in silicon photonic crystal slabs," *Applied Physics Letters*, Vol. 94, No. 15, 154104, 2009.

[11] Li, S., H. Liu, Q. Sun, and N. Huang, "A tunable terahertz photonic crystal narrow-band filter," *IEEE Photonics Technology Letters*, Vol. 27, No. 7, 752–754, 2015.

[12] Chen, T., Z. Han, J. Liu, and Z. Hong, "Terahertz gas sensing based on a simple one-dimensional photonic crystal cavity with high-quality factors," *Applied Optics*, Vol. 53, No. 16, 3454–3458, 2014.

[13] Li, H., W. Xue, N. Li, Y. Du, and C. Li, "Mode characteristics of a graphene-coated cylindrical dielectric waveguide with a nested eccentric hollow elliptical cylinder," *Journal of the Optical Society of America B*, Vol. 39, No. 11, 2944–2956, 2022.

[14] Liu, C.-M. and K. Wu, "Vertically stacked double-layer substrate-integrated nonradiative dielectric waveguides for THz applications," *IEEE Microwave and Wireless Technology Letters*, Vol. 33, No. 6, 791–794, 2023.

[15] Bhat, Z. A., J. A. Sheikh, R. Rehman, S. D. Khan, I. Bashir, and S. Ashraf, "A survey on substrate integrated waveguide filters; design challenges and miniaturizing techniques for the 5G," *International Journal of High Speed Electronics and Systems*, Vol. 32, No. 01, 2140006, 2023.

[16] Gomez, A., M. A. Solano, A. Lakhtakia, and A. Vegas, "Circular waveguides with Kronig-Penney morphology as photonic bandgap filters," *Microwave and Optical Technology Letters*, Vol. 37, No. 5, 316–321, 2003.

[17] Alfihed, S., M. H. Bergen, A. Ciocoiu, J. F. Holzman, and I. G. Foulds, "Characterization and integration of terahertz technology within microfluidic platforms," *Micromachines*, Vol. 9, No. 9, 453, 2018.

[18] Lee, I.-S. and J. W. Lee, "Nondestructive internal defect detection using a CW-THz imaging system in XLPE for power cable insulation," *Applied Sciences*, Vol. 10, No. 6, 2055, 2020.

[19] Xie, J., W. Ye, L. Zhou, X. Guo, X. Zang, L. Chen, and Y. Zhu, "A review on terahertz technologies accelerated by silicon photonics," *Nanomaterials*, Vol. 11, No. 7, 1646, 2021.

[20] Wen, W., W. Yan, C. Lu, L. Lu, X. Wu, Y. Lu, S. Zhu, and X.-S. Ma, "Polarization-entangled quantum frequency comb from a silicon nitride microring resonator," *Physical Review Applied*, Vol. 20, No. 6, 064032, 2023.

[21] Lai, N. D., J. H. Lin, Y. Y. Huang, and C. C. Hsu, "Fabrication of two-and three-dimensional quasi-periodic structures with 12-fold symmetry by interference technique," *Optics Express*, Vol. 14, No. 22, 10 746–10 752, 2006.

[22] Konoplev, I. V., A. J. MacLachlan, C. W. Robertson, A. W. Cross, and A. D. R. Phelps, "Cylindrical, periodic surface lattice — Theory, dispersion analysis, and experiment," *Applied Physics Letters*, Vol. 101, No. 12, 121111, 2012.

[23] Touiss, T., S. Machichi, Y. Errouas, I. E. Kadmiri, F. Falyouni, and D. Bria, "Comparative study of photonic defective comb-like structure by the green function and the transfer matrix method," in *E3S Web of Conferences*, Vol. 469, 00044, EDP Sciences, 2023.

[24] Touiss, T., I. E. Kadmiri, Y. Errouas, and D. Bria, "Electromagnetically induced transparency and fano resonances in waveguides and U-shaped or cross-shaped resonators," *Progress In Electromagnetics Research M*, Vol. 127, 53–63, 2023.

[25] Khattab, M. S., T. Touiss, I. E. Kadmiri, F. Z. Elamri, and D. Bria, "Multi-channel electromagnetic filters based on EIT and Fano resonances through parallel segments and asymmetric resonators," *Progress In Electromagnetics Research Letters*, Vol. 115, 105–109, 2023.

[26] Touiss, T., Y. Errouas, I. E. Kadmiri, and D. Bria, "Electromagnetic filtering with high performance by one dimensional defective comb-like waveguides structure using the transfer matrix," in *E3S Web of Conferences*, Vol. 469, 00091, EDP Sciences, 2023.